SSRG International Journal of Electronics and Communication Engineering
ISSN: 2348-8549/ https://doi.org/10.14445/23488549/IJECE-V11I4P113

Volume 11 Issue 4, 121-132, April 2024

Original Article

Performance Analysis of Bismuth-Based $CsBi_3I_{10}$ Tandem Perovskite Solar Cell

Shreyus Goutham Kumar[1], H.G. Abhigna[2], N. Sindhu[2], C.R. Prashanth[3]

[1]*Department of Electronics and Telecommunication Engineering, Dr. Ambedkar Institute of Technology, Karnataka, India.*
[1,2]*Department of Electronics and Communication Engineering, PES University-EC Campus, Karnataka, India.*
[3]*Department of Electronics and Communication Engineering, SJB Institute of Technology, Affiliated to VTU, Karnataka, India.*

[1]*Corresponding Author : shreyasgouatham@pes.edu*

Received: 14 February 2024 Revised: 15 March 2024 Accepted: 12 April 2024 Published: 30 April 2024

Abstract *- With the ever-increasing energy demands, the quest for renewable energy has led to the exploration of inorganic perovskite solar cells having a higher efficiency of more than 25.5%. The full solar spectrum is exploited to achieve a higher power conversion efficiency to surpass the Shockley-Queisser limit. Using SCAPS-1D, this work simulates single and tandem solar cells. This simulation features a $CsBi_3I_{10}$ perovskite absorber layer sandwiched between the electron transport layer (ETL) and hole transport layer (HTL). The standalone cell achieved a Power Conversion Efficiency (PCE) of 21.6%, a fill factor of 82.2%, J_{sc} of 20.9 mA/cm^2, and V_{oc} of 1.25 V. To bypass the Shockley-Queisser limit, the solar cell is integrated into the crystalline silicon solar cell by mechanically stacking on top of each other. Tandem cells achieved a power conversion efficiency of 30.8%, higher than a single cell. The paper discusses the impact of choosing different combinations of ETL and HTL layers. According to the simulation, $CuSbS_2$ and SnO_2 are the best combinations for HTL and ETL. Apart from single and tandem cell performance analysis, the paper explores the effect of the absorber layer's thickness, bandgap, and defect density, along with ETL and HTL thickness. A Tandem solar cell with $CsBi_3I_{10}$ and the efficiency by the tandem configuration is 30.8% (FF=77.69%, J_{sc}=13.5 mA/cm^2, V_{oc}=1.77 V).*

Keywords *- Perovskite solar cells, Tandem devices, SCAPS 1-D, Power conversion efficiency, Lead-free, Fill-Factor.*

1. Introduction

Energy demand has increased dramatically over the past century [1]. Estimates suggest that this demand could double in the next few decades. Right now, mainly fossil fuel is used to run economies, CO_2 emissions from burning fossil fuel from the industrial and automobile sectors not only hurt the environment but also are a major contributor to global warming and climate change. Countries around the world are taking steps at a fast pace to reduce carbon emissions.

One of the major ways to reduce carbon accumulation in the atmosphere is to adopt renewable and clean sources of energy. Clean energy technologies, especially photovoltaic technologies, show great promise in the industrial sector due to their ability to generate clean energy, harness sunlight for carbon-free electricity, and operate efficiently over extended periods without requiring much maintenance. For wider adoption of solar technology, a great advancement in solar efficiency and reduced cost is the main focus of the solar energy community. As a result, a newer generation of solar absorber material called perovskite has come under the radar of researchers due to its unique higher efficiency and reduced cost.

The general structure of perovskite is ABX_3 having a cubic structure, where A is an active formamidinium ($CHNH^{+3}$ = NH) ion or an organic counterpart such as methyl ammonium ($CH3NH^{+3}$) ion occupying the body center position of the crystal. B represents inorganic cations such as Sn^{+2} or Pb^{+2} occupying the corners, and X generally refers to the halogen ions Cl^-, Br^-, and I^- occupying the face center of the crystal. The perovskite structure is very much susceptible to degradation when exposed to moisture, heat, and light which can limit their long-term usage.

The solar cell research community had shown a great interest in lead-based perovskite solar cells, which delivered a great efficiency of 26.1% and good air stability. However, due to the toxic nature of lead, it becomes a challenge to scale the production employing lead as an absorber material since it can degrade and easily contaminate the local water body, soil and dust, thereby affecting not only the ecosystem but also human health.

Lead poisoning leads to long-term health issues, including kidney damage, cardiovascular problems, and nervous damage. In pregnant women, exposure to high levels

of lead might lead to miscarriage, stillbirth, premature birth, and low birth weight. So, it becomes a major reason to shift from lead to a non-lead-based solar cell for wider adoption, ease of manufacturing, reduced cost, and safety.

Today's solar cells primarily use silicon, which has been used for many decades. Silicon solar cells are considered the 'first generation' cells and came into importance in the 1950s. Bandgap energy of 1.12eV of crystalline silicon (c-Si) stands out among photovoltaic materials as one of the most important candidates for the development of multijunction cells due to its adequate bandgap, high efficiency, competitive price, non-toxic nature, and exceptional stability.

In the current photovoltaic market, crystalline silicon (Si) solar cells offer more than 25% efficiency [2]. However, the major drawback of c-Si-based photovoltaics is that the manufacturing process involves a large amount of energy expenditure and uses a lot of water and toxic chemicals. To overcome the drawback, nonlead perovskite is a potential option for wide market adoption.

Due to several advantageous properties such as tunable bandgaps, extended carrier diffusion length, reduced carrier effective mass, good absorption coefficient, cost-effectiveness, and straightforward fabrication, perovskite materials have emerged as promising routes for two junction-solar cells (TSCs). In 2015 Mailoa et al. were the first to synthesize the first double-ended (2-T) perovskite/Si TSC that gave a photoelectric conversion efficiency (PCE) of 13.7%. On top of this, Zheng et al. The structure was improved by adding SnO_2 as both the electron transport layer (ETL) and the interconnecting layer (ICL) of the surface cell. This modification increased PCEs, reaching 17.10% at 16 cm^2 TSC.

This paper presents a simulation study of Cesium Bismuth Iodide ($CsBi_3I_{10}$), considering it as an absorber layer with novel ETL and HTL configuration, comparing it with the existing configuration, and analyzing how the variation of parameters impacts the overall performance of the solar cell. To surpass the Shockley-Queisser limit, the standalone cell is paired with a crystalline silicon solar cell, this configuration is termed as a tandem structure. The short circuit current of the top cell and bottom cell is matched to be the same by adjusting the thickness of the layers to ensure the correctness of the device simulation.

2. Device Structure

The general structure of a solar cell consists of a conductive glass substrate, electron transport material, absorber layer, hole transport material, and silver or gold back contact consisting of the top cell only. However, when considering a 2 terminal tandem, it consists of a top cell and a c-Si bottom cell simulated separately. The traditional muti-junction modeling approach assumes that the tunnel junction is fault-free, and the model ignores both optical and electrical losses occurring at the interfaces [3]. Solar cells made up of perovskite are considered top cells, and crystalline silicon solar cells as bottom structures (highly stable) are used in tandem solar cell architecture.

In this simulation, the top cell $CsBi_3I_{10}$ (Bandgap: 1.75 eV, Thickness: 1000 nm) is an absorber sandwich between an Electron Transport Layer (ETL) and a hole transport material (HTL). Looking into the potential candidates for ETL material, SnO_2 and HTL material, $CuSbS_2$ are considered.

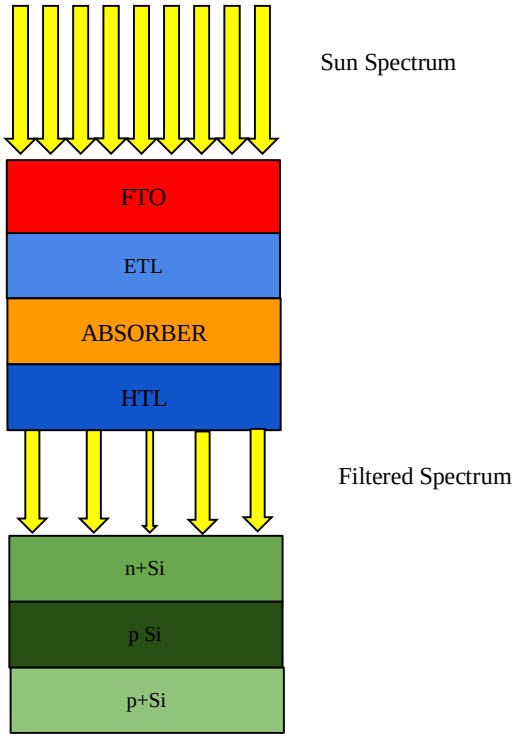

Fig. 1 Tandem solar cell structure

3. Methodology

Developed by the University of Gent's Department of Electronics and Information Systems, SCAPS (Solar Cell Capacitance Simulator) is a powerful tool for simulating the behavior of one-dimensional solar cells. Initially designed for $CuInSe_2$ and CdTe cell structures, SCAPS has evolved to encompass crystalline (Si and GaAs) and amorphous (a-Si and micro amorphous Si) solar cells."

Tandem structures are the new field of exploration, trying to surpass the Shockley-Queisser limit of 33% efficiency mark. The combination of silicon with III-V group materials, CZTS(copper, zinc, tin, sulfide), CIGS(copper, indium, gallium, selenide), perovskites and polymers in tandem architecture shows promising results in the field of renewable solar technology. This approach is called tandem/ multi-junction solar cell, it aims to increase the efficiency by combining materials with complementary absorption spectra.

The procedure for simulating a tandem involves splitting the tandem into two separate diodes and simulating the top cell with the AM1_5G 1 sun spectrum and the bottom cell with the filtered spectrum (using eq no 1) separately; this procedure is followed due to the limitation of the tool to model the multi-junction solar cell [4].

$$S(\lambda) = S_0 \cdot exp(\sum_{i=1}^{4} -\alpha_{mat_i}(\lambda) d_{mat_i}) \quad (1)$$

S(λ) is the filtered power spectrum, and the sun power spectrum is denoted by So, d_{mat_i} is the layer thickness in cm, $\alpha_{mat_i}(\lambda)$ is the absorption coefficient of layers (using eq 2) given by [4],

$$\alpha(E) = A_a \cdot \sqrt{h\nu - E_g} \quad (2)$$

A_a given by 10^5 $cm^{-1}eV^{-1/2}$ [5], plank's constant denoted by H. Frequency ν in $sec^{-1,}$ and the bandgap represented by E_g respective layers.

Certain factors that characterize the electrical, optical, and physical properties of semiconductors are essential material features for solar cell simulations with programs like SCAPS. One of these characteristics is the bandgap (Eg), which is essential for figuring out how much of the solar spectrum a material can absorb and transform into electrical energy [6]. Understanding how a semiconductor behaves in an electric field and interacts with light requires knowledge of the electron affinity (χ) and the dielectric constant (ε) [7].

The effective masses of electrons and holes, along with the density of states in the conduction and valence bands, have an impact on the carrier dynamics and the semiconductor's potential to conduct electric current.[8].

The efficiency of the device is affected by carrier mobility (μe and μh), which measures how fast carriers can pass through the material]. The purity and inherent charge carrier density of the semiconductor are indicated by the temperature-dependent intrinsic carrier concentration (ni). When designing the active layer of solar cells to maximize light absorption, the absorption coefficient (α)-which describes how the material absorbs light-is crucial [9]. N_A, $N_{D,}$ and N_t denote doping concentrations and defect states in semiconductor materials. Acceptor impurities, represented by Na, produce holes as majority carriers, whereas donor impurities, represented by Nd, supply free electrons. Within the semiconductor's band gap, Nt stands for trap states or defect levels that have the potential to trap free carriers and impact device efficiency.

The device's total efficiency is also influenced by the parameters that describe how long carriers can contribute to current before recombining: surface recombination velocities and lifetime of electrons and holes (τ_n and τ_p) 10]. For precise simulation and optimal design of solar cells, certain material attributes are essential. Each one contributes differently to the efficiency and performance of photovoltaic devices. Scientists and engineers can forecast how solar cells will behave in different scenarios by comprehending and precisely adjusting these parameters in simulation environments.

Table 1. Reference device parameters

Parameter	ITO	CeOx	$CsBi_3I_{10}$	NiOx
Thickness (nm)	50	100	1000	400
Eg [eV]	3.6	3.5	1.75	3.8
χ [eV]	4.5	4.4	4.2	1.46
εr	8.9	9	10	10.7
N_c [cm^{-3}]	2.2 x 10^{18}	1 x 10^{20}	2.2 x 10^{18}	2.2 x 10^{18}
N_v [cm^{-3}]	1.8 x 10^{19}	2 x 10^{21}	1.8 x 10^{19}	1x 10^{19}
μ_e [cm^2 VS^{-1}]	10	100	2	12
μ_h [cm^2 VS^{-1}]	10	25	2	2.8
N_D [cm^{-3}] Donor density	10^{21}	10^{21}	0	0
N_A [cm^{-3}] Acceptor density	0	0	10^{15}	10^{21}
N_t	-	10^{14}	10^{14}	10^{21}

Table 2. Parameters for ETL material

Parameter	WS_2	IGZO	TiO_2	SnO_2	PCBM
E_g [eV]	1.8	3.05	3.2	3.3	2
χ [eV]	3.95	4.16	4.26	4	3.9
ε_r	13.6	10	10	9	3.9
N_c [cm^{-3}]	$1x10^{18}$	$5x10^{18}$	$2.2x10^{18}$	2.2×10^{17}	$2.5x\ 10^{21}$
N_v [cm^{-3}]	$2.4x10^{19}$	$5x10^{18}$	$1.8x10^{19}$	$2.2x\ 10^{16}$	2.5×10^{21}
μ_e [$cm^2\ VS^{-1}$]	100	15	100	200	0.2
μ_h [$cm^2\ VS^{-1}$]	25	0.1	25	80	0.2
N_D [cm^{-3}]	$1x10^{15}$	$1x10^{17}$	$1x10^{19}$	$1x10^{17}$	2.93×10^{17}
N_A [cm^{-3}]	0	0	0	0	0
N_t	$1x10^{15}$	$1x10^{15}$	$1x10^{15}$	$1x10^{14}$	$1x10^{15}$

Table 3. Parameters for HTL material

Parameters	Cu_2O	$CuSbS_2$	NiO	CFTS
E_g [eV]	2.98	1.58	3.8	1.3
χ [eV]	2.1	4.2	1.46	3.3
ε_r	6.5	14.6	11.7	9
N_c [cm^{-3}]	$2.8x10^{19}$	$2x10^{19}$	$2.5x10^{15}$	$2.2x10^{18}$
N_v [cm^{-3}]	$1x10^{19}$	$1x10^{19}$	$1.8x10^{18}$	$1.8x10^{19}$
μ_e [$cm^2\ VS^{-1}$]	80	49	0.02	21.98
μ_h [$cm^2\ VS^{-1}$]	80	49	0.0002	21.98
N_D [cm^{-3}]	0	0	0	0
N_A [cm^{-3}]	$1x10^{18}$	$1.38x10^{18}$	3.17×10^{14}	$1x10^{18}$
N_t	$1x10^{15}$	$1x10^{14}$	$1x10^{15}$	$1x10^{15}$

The outcome derived from the above reference for the ITO/CeOx/CsBi3I10/NiOx/Au architecture are, Voc=1.29V, Jsc=16.32mA/cm2, FF=84.7%, PCE=17.82 % [10].

To improve the overall performance of the perovskite cell, different HTL materials such as $CuSbS_2$, CFTS, NiO, and Cu_2O [11-14] and ETL materials like TiO_2, WS_2, SnO_2, IGZO, and PCBM [15-17]are being experimented with. Table 2 and Table 3 provide specific parameter values for various materials.

It is used to model a photovoltaic device and analyze its Open circuit voltage (Voc), Fill factor (FF), Short circuit current density (Jsc) and Power conversion efficiency (PCE). The performance parameters are evaluated by using the continuity equation by solving Poisson's equation.

$$\frac{d}{dz}[-\varepsilon(z)\frac{d\emptyset}{dz} = q[p(z) - n(z) + N_D^+(z) - N_A^-(z) + p_t(z) - n_t(z)] \quad (3)$$

$$\frac{dp_n}{dt} = G_p - \frac{p_n - p_{n0}}{\tau_p} + p_n\mu_p\frac{d\xi}{dz} + \mu_p\xi\frac{dp_n}{dz} + D_p\frac{d^2p_n}{dz^2} \quad (4)$$

$$\frac{dn_p}{dt} = G_p - \frac{n_p - n_{p0}}{\tau_n} + n_p\mu_n\frac{d\xi}{dz} + \mu_n\xi\frac{dn_p}{dz} + D_p\frac{d^2n_p}{dz^2} \quad (5)$$

It is important to keep in mind that only solar cells absorb photons with energy higher than the semiconducting material's band gap [1]. The least wavelength of the photon which can generate electron and hole pair is determined by bandgap Eg, the cutoff wavelength is determined by

$$\lambda = \frac{1240}{E_g(eV)} \quad (6)$$

When the short circuit current density (Jsc) = 0 $mAcm^{-2}$, The highest voltage generated by the solar cell is called the open circuit voltage(Voc), given by

$$V_{oc} = \frac{kT}{q} ln\left(\frac{J_{sc}}{J_0} + 1\right) \quad (7)$$

Where J_0 is the saturation point current density, T is the temperature, q is the carrier charge, and K is the Boltzmann constant. The fill factor is determined by [18].

$$FF = \frac{P_m}{V_{oc} \times J_{sc}} \quad (8)$$

The optimized fill factor is given by Equation 9.

$$FF = \frac{v_{oc} - ln(v_{oc} + 0.72)}{v_{oc} + 1} \quad (9)$$

v_{oc} is the normalized form of V_{oc}, and is given by Equation 10.

$$v_{oc} = \left(\frac{V_{oc}}{V_{th}}\right) \quad (10)$$

The maximum power point is a symbolic representation of the ideal balance between power output and power input for a solar cell which is given by Equation 11.

$$\eta = \frac{P_m}{P_{in} \times A} \quad (11)$$

The amount of radiation at which it reaches the surface is known as Pin and is represented by A for area. Furthermore, it should be noted that when a solar cell has a voltage of zero, the short-circuit current is directly linked to the electricity passing through the cell. This particular current is both provided and influenced by the solar spectrum at play.

$$J_{sc} = q\int_{E_g}^{\infty}\frac{dN_{ph}}{dhv}d(hv) \quad (12)$$

The relationship in Equation 13 offers a comprehensive understanding of bandgap changes based on the temperature, T, at any given time.

$$E_g(T) = E_g(0) - \frac{\alpha T^2}{(T+\beta)^2} \quad (13)$$

The constants α and β are primary factors that determine the short-circuit current (J_{sc}). The electron mobility has a significant impact on J_{sc}, and adjusting the material's properties can alter the material-dependent electron affinity, which also plays a vital role.

4. Results and Discussion

4.1. Results and Validation

Figure 1 illustrates the construction of the perovskite solar cell utilizing $CuSbS_2$ and SnO_2 as the HTL and ETL components, respectively, as described in Section 2. In the subsection that follows, the solar cell is optimized by choosing appropriate electron and hole transport layers, adjusting the thickness of the absorber layer and bandgap, investigating the effects of defect densities in the absorber layer on performance, optimizing ETL and HTL thickness to harness the best performance. The outcomes of the optimized architecture, which uses $CuSbS_2$ as the HTL material and SnO_2 as the ETL, are compared with the reference architecture in Table 4.

Table 4. Device parameter comparison of $CsBi_3I_{10}$

Architecture	V_{oc}	J_{sc}	FF	PCE
ITO/CeO_x/$CsBi_3I_{10}$/Ni O_x/Au [10]	1.29	16.32	84.7	17.82
FTO/SnO_2/$CsBi_3I_{10}$/$CuSbS_2$/Au (Proposed Structure)	1.25	20.9	82.2	21.6

According to experimental results, the maximum PCE in a solar cell with $CsBi_3I_{10}$ as the perovskite layer is 0.84% [11, 19, 20]. On the other hand, [10] reports an efficiency of 17.82 in simulation, which is the highest among the reported works.

4.2. Selection of Best ETL Material and Its Impact on Cell Performance

The modeling results for the perovskite solar cells using different ETL materials are shown in Table 5. Table 5 gives the reference HTL (NiO), which is fixed. With a 21.3% efficiency, SnO_2 produced the highest results. The main selection criteria for the ETL layer depends on the band alignment between the absorber, ETL and FTO. The general tendency of the electron is to move from a higher energy conduction band to a lower energy conduction band. The SnO_2 gives the best efficiency since the performance of the cell not only depends on the band energy but also the thickness, and electron mobility as well and SnO_2 has the highest mobility compared to any other material. Also The

conduction band minimum of the conducting surface FTO's band gap should be considered having -3.8 to -4.2 eV. The configuration considering SnO_2 gives the best efficiency and J_{sc}.

Table 5. Results of PSCs with various ETL materials

Results	SnO_2	WS_2	TiO_2	IGZO	PCBM
V_{oc} (V)	2.626	3.242	1.345	2.603	2.319
J_{sc}(mA/cm^2)	19.75	18.88	17.91	19.755	19.145
FF (%)	36.61	29.36	74.94	36.90	40.97
PCE (%)	18.99	17.97	18.06	18.98	18.2

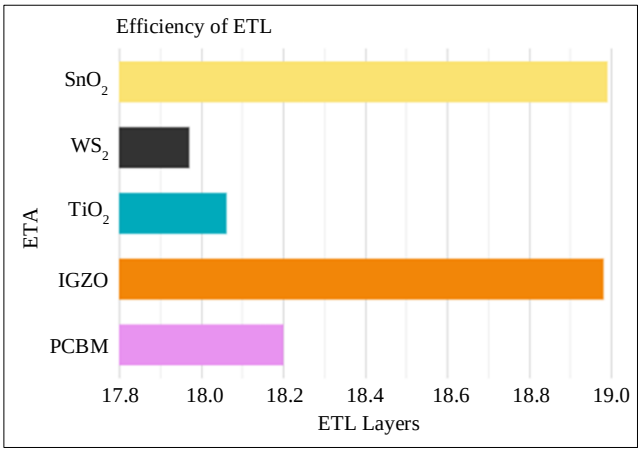

Fig. 2 Efficiency chart of HTL layers

4.3. Selection of Best HTL Material and Impact on Cell Performance

Since SnO_2 returned the highest efficiency concerning the absorber material, SnO_2 is kept constant and the solar cell is simulated with various HTL materials with the parameters given in Table 3. The results of the simulation are depicted in Table 6 and Figure 3. It is observed from the simulation that $CuSbS_2$ returned the highest efficiency of 21.6%. Table 6 shows that the most PCE is obtained with $CuSbS_2$ HTL, and the least PCE is obtained with CFTS when utilized as HTL. $CuSbS_2$ returns the highest efficiency for the solar cell, where high hole mobility and thickness have a definite impact on the performance.

4.4. Effect of Absorber Layer Thickness on Performance

The thickness of the absorber layer plays an important role in the performance of solar cells. A balance between simulation thickness and real-world practicality is needed. Thus, choosing the optimum thickness to maximize the photon conversion and minimize the reverse saturation current is important. In an experimental setup where all other parameters were constant, the absorber layer thickness was systematically varied in the range of 100 nm to 1000 nm. The corresponding variable parameters were meticulously recorded. This systematic exploration allows for a comprehensive understanding of how the absorber layer thickness influences key aspects of solar cell performance, aiding in identifying the thickness that yields optimal results.

Table 6. Results of PSCs with various HTL materials

Response	Cu_2O	NiO	CFTS	$CuSbS_2$
V_{oc} (V)	1.14	2.621	0.59	1.24
J_{sc} (mA/cm^2)	19.01	19.75	33.59	19.95
FF (%)	73.7	36.61	53.22	82.2
PCE (%)	16.11	18.99	10.55	20.5

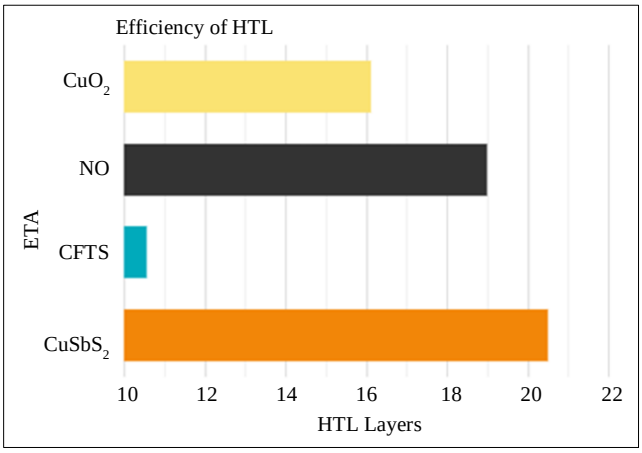

Fig. 3 Effect of various HTL layers

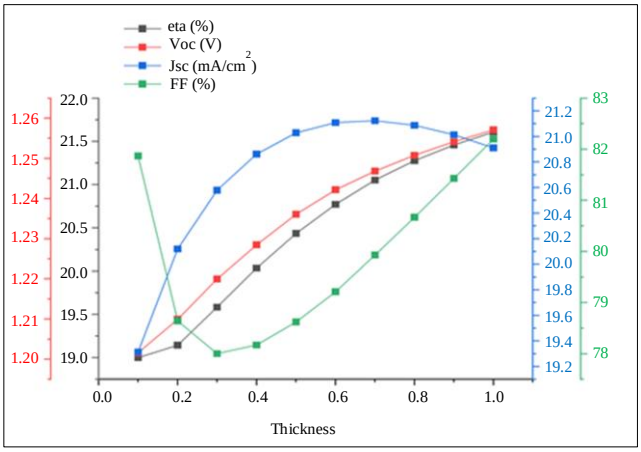

Fig. 4 Effect on (a)Voc, (b)Jsc, (c) ETA, and (d) FF due to thickness variation.

The efficiency of the cell increases in an approximately linear fashion, as shown in Figure 4; as the absorber layer thickness increases, it captures more incoming photons, resulting in an increase in PCE and Jsc. FF decreases initially;

it might be due to the increased series resistance of the material, but as thickness increases, more number of photons are absorbed, and the FF increases.

4.5. Effect of Variation in the Band Gap of the Absorber Layer

To enhance device efficiency, optical deflection control through energy gap variation in deflecting elements is crucial. From the simulated results presented in Figure 4 1.75eV is the ideal band gap for high efficiency, as in the graph. It is observed that with the increase in the band gap, the PCE decreases. Therefore, the absorber layer's band gap to choose from is 1.75eV by maintaining a fixed $CsBi_3I_{10}$ thickness at 1000 nm, yielding a maximum PCE of 21.6% and a maximum FF of 82.2%.

From Figure 5, it is visible that as the bandgap increases, the efficiency and Jsc parameter decrease; when the bandgap increases, only the photons with energy greater than the work function (band gap) of the material can generate electron and hole pair.

As a result, the increase in the bandgap and the number of e-h pairs generated drastically reduces, thereby affecting photon conversion efficiency and Jsc. Whereas the impact of increasing the Bandgap has a limited effect on the open circuit voltage due to the higher band gap, the recombination rate increases; as a result, there is a slight decrease in Voc.

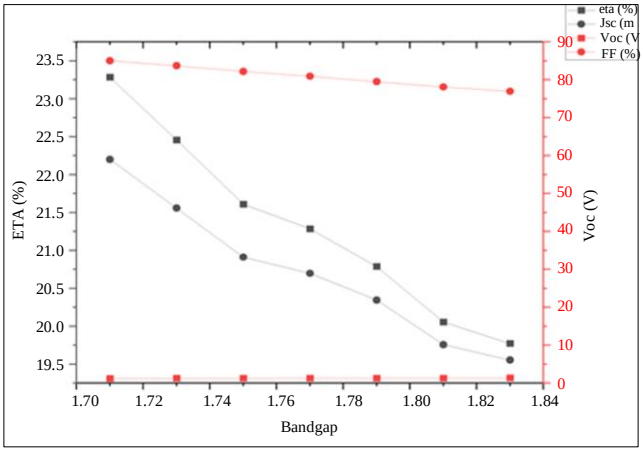

Fig. 5 Effect on (a) PCE, (b) Voc, (c) Jsc, and (d) FF due to band gap variation.

4.6. Effect of Variation in Absorber Layer Electron Affinity

The electron affinity of the material is the required energy to convert a neutral atom into a negative ion. In the context of Perovskite Solar Cells (PSCs), the electron affinity of the material affects the device performance, and it is one of the important parameters to be taken care of. To assess the impact of electron withdrawal in $CsBi_3I_{10}$ on PSC characteristics, a range of 3.8 to 4.8 eV was explored.

Furthermore, a slight increase in power conversion efficiency (PCE) from 21.6% to 22.9% was observed from 4.2 to 4.4eV and a sudden decrease in efficiency to 0.443% at 4.6 ev. Optimizing electron absorption from the adsorbent layer is essential for achieving optimal PSC performance. Figure 6 depicts the effect of electron affinity on key aspects of solar cell performances.

From Figure 6, Voc has minimal change with an increase in electron affinity. The open circuit voltage is mainly dependent on the bandgap. However, with an increase in e-affinity, there is a possibility that the generated electrons might recombine at the absorber and HTL interface, thereby decreasing Voc. It is also imperative from the graph that Jsc only increases up to a certain point and drastically falls, which shows that when the value of electron affinity crosses 4.4 eV, the surface recombination is dominant, and Jsc is reduced.

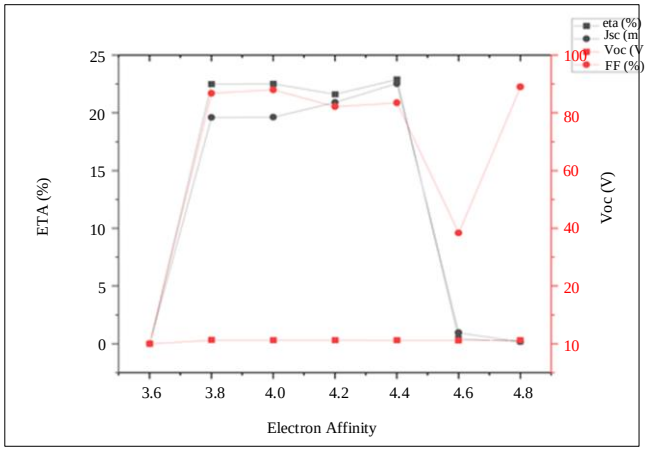

Fig. 6 Effect on (a) ETA, (b) Voc, (c) Short circuit current, and (d) FF.

4.7. Impact of Absorber Layer Defect Density

All perovskite materials inherently exhibit defects, including point defects like vacancies, gaps, and Schottky and Frenkel defects. Additionally, reflections and grain boundaries may occur on surfaces, and impurity defects may arise from self-doping methods, trapping charge carriers and encouraging nonradiative recombination. High defect densities adversely impact the performance of perovskite solar cells (PSCs). To assess the impact of absorber layer (AL) defect density, it was varied from 10^{13} to 10^{17} cm^{-3}. Figure 7 indicates that Voc, Jsc, ETA and FF decrease with increasing defect density, as shown in Figure 7.

Defects are the major hindrance for any type of solar cell, the performance of the cell drastically reduces with an increase in defects. Defects act as recombination centers where the electron loses out energy and falls back to its ground state. This hinders the lifespan of the generated carriers and reduces the overall performance of the solar cell. From Figure 7, with an increase in defects, all the parameters decrease drastically.

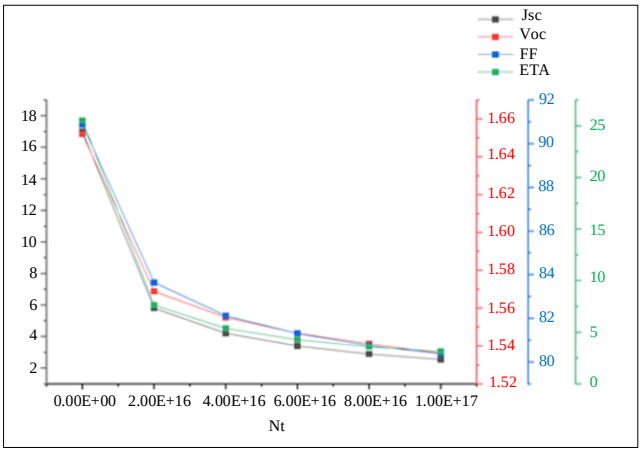

Fig. 7 Effect on (a) Voc, (b) Jsc, (c) PCE, and (d) FF.

4.8. Effect of ETL Thickness

The thickness of the Electron Transport Layer (ETL) is crucial for device performance, serving as an electron transfer pathway. Varying ETL size affects series resistance, impacting charge separation. So, therefore, varied the thickness from 30 nm to 150 nm and observed that there is no crucial impact of ETL thickness on the device from Figure 8.

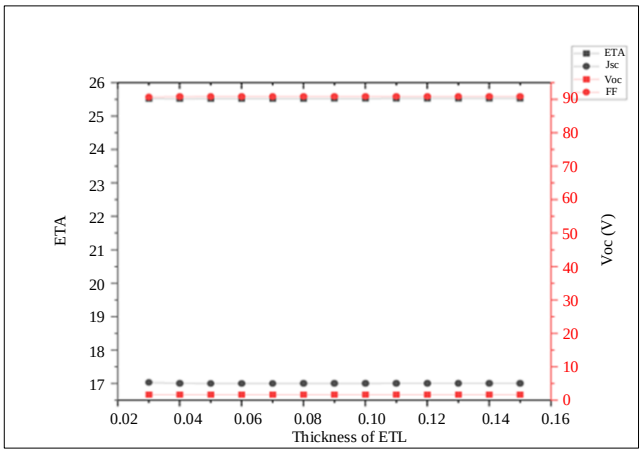

Fig. 8 Denotes the effect on (a)Voc, (b) Jsc, (c) ETA, and (d) FF.

4.9. Impact of HTL/Absorber Interface Defect Density

When two materials don't fit structurally or when impurities from the environment get inside PSCs, interfacial defects-also referred to as charge recombination centers-form [19]. Third-generation solar cells-more especially, those made from solutions-have a significant impact on the processing method. Non-radiative losses also result from defects in the perovskite absorber and low electrical quality in the heterojunctions between the charge extraction layer (ETL) and the perovskite, which generates the Voc loss [21].

The device's long-term stability and performance are impacted by the interactions between the multiple PSC levels. Voltage and current are lost during trap-assisted non-radiative recombination if an interface with numerous defects/voids or trap states is used. To comprehend the impact of defect density at the HTL/absorber layer interface, a value that falls between 10^{10} and 10^{21} cm^{-3} is chosen. Figure 9 below illustrates the significantly less effect of the defect density of the HTL/AL interface on PSC performance.

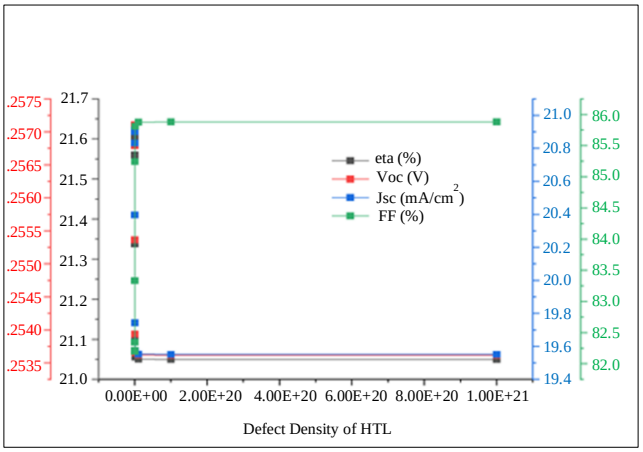

Fig. 9 Effect on (a) FF, (b) Jsc, (c) Voc, and (d) ETA.

4.10. Effect of Defect Density of ETL/Absorber Interface

In comparison to rear interface faults, front interface defects have a greater impact on a PSC device's performance. Perovskite materials' high absorption coefficient, which increases photon absorption close to the front contact, explains this behavior. Numerous electron-hole pairs are thus produced in the vicinity of the front contact. Now it is known that the ratio of trap-assisted recombination to charge carriers. The fact that front interface issues influence the device's functionality to a great extent should be noted. Therefore, the front interface must be fault-passivated with care. In terms of PSC performance, it was found that ETL/AL interface defect density has a much smaller impact. Various metrics have demonstrated these effects (See Figure 10).

4.11. Carrier Density Impact on Device Performance

4.11.1. Impact of HTL Defect Density

There are two ways in which one can dope ETL and HTL. Minority carriers are able to achieve this, but the photovoltaic properties are significantly diminished in the process. However, it is possible to obtain most carriers with significantly better PV properties. A medium doping density will help to enhance PSC performance. They have performed device simulations for a range of acceptor densities, from 10^{17} to 10^{22} cm^{-3}, to obtain this optimal density. From Figure 11, it can be shown that the change of Jsc and Voc is inconsequential concerning the acceptor density of HTL, while there may be slight linear increments for Jsc and Voc. FF and PCE curves, respectively, rise from 81.8 to 86.2% and 21.4 to 26.3%.

The higher the NA, therefore, the greater the electrostatic potential established at the electric interface between these

layers, thereby enhancing both charge separation within this PSC (thereby improving its photoconversion efficiency) and slowing down carrier recombination [22]. Therefore, from Figure 11, It is also interesting to note that an increase in the dopant concentration above optimum leads to a decrease in bulk mobility due to deep coulomb traps, which will lower an overall performance; hence, 10^{22} cm^{-3} is considered as an optimal value for acceptor density [23].

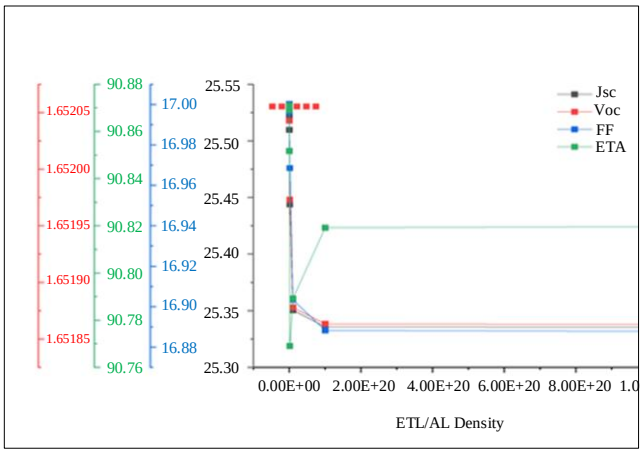

Fig. 10 Effect on (a) FF, (b) Jsc, (c) Voc, and (d) ETA.

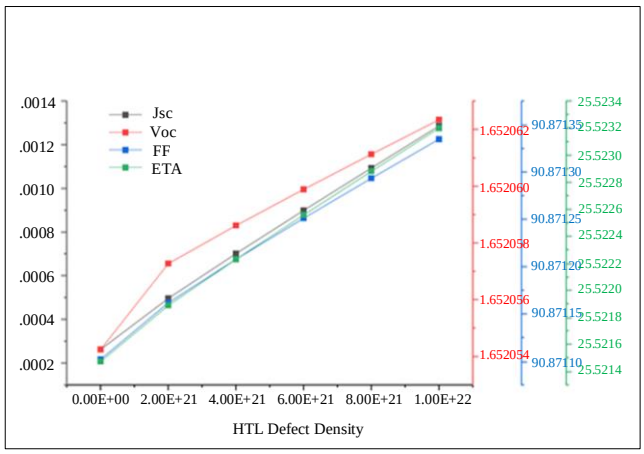

Fig. 11 Effect on (a) FF, (b) Jsc, (c) Voc, and (d) ETA.

4.11.2. Impact of ETL Acceptor Density

Figure 12 denotes the varying effect of ETL donor density on device performance. They have varied Nd from 10^{15} to 10^{19} cm^{-3} such that some optimal Donor density could be obtained in light of the more efficient parameters already optimized in prior sections. This can be concluded from the fact that Jsc, Voc, and FF are approximately constant throughout, which also means that PCE is not affected by variation in Nd, as shown in Figure 12.

4.12. Impact of Variation in Back Contact Work Function

The work function of the back contact is nothing but the amount of energy required to remove an electron and displace it in a vacuum. The work function of the material depends upon various factors and varies from metal to metal. Gold is considered the best contact material for back contact due to its unique property of high conduction and it reflects the photons back to the absorber layer. In the simulation, keeping all the parameters constant the work function of the material is varied from 5 eV to 6eV.

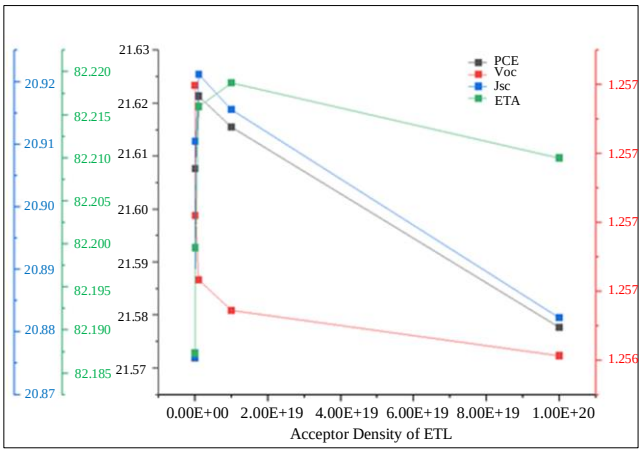

Fig. 12 Effect on (a) FF, (b) Jsc, (c) Voc, and (d) ETA.

As shown in Figure 13, an increase in work function has minimal impact on the short circuit current up to 5.8eV because the work function has created a sufficient barrier for efficient hole extraction. After crossing the mark of 5.8 eV, there is a steep rise in short circuit current; this might be attributed to a possible change in the hole extraction mechanism, which needs further investigation into the matter.

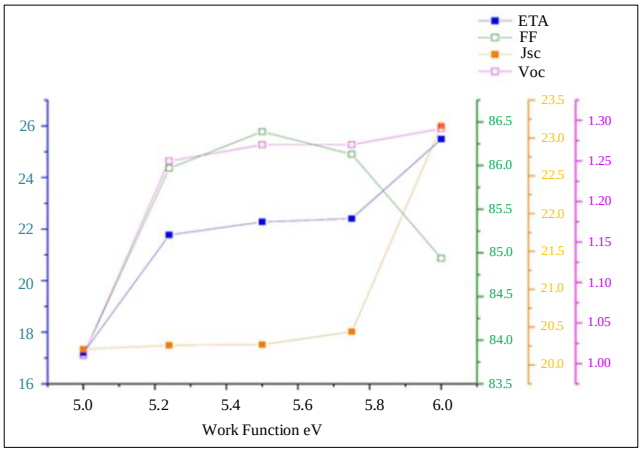

Fig. 13 Effect of increasing work function on device performance

5. Simulation of Bottom Cell (c-Si)

A crystalline-Si solar cell is considered a bottom cell in tandem simulation. A synchronized current matching state is crucial for the efficient functioning of tandem solar cells [24, 25]. This means ensuring uniform electrical properties across individual cells, as it greatly impacts the conversion of absorbed light into electrical energy for each layer.

To meet this requirement, adjustments can be made to layer thickness, doping levels, and material composition to align electrical resistance and open circuit voltage between cells. The following Table 7 shows the parameters that are used to simulate the bottom cell. With their ability to achieve elevated conversion efficiencies, tandem solar cells hold great promise for renewable energy production.

Table 7. c-Si bottom solar cell device parameters

Parameter	p+Si	pSi	n+Si
Thickness (µm)	0.1	10	1.61
E_g [eV]	1.12	1.12	1.12
χ [eV]	4.05	4.05	4.05
ε_r	11.9	11.9	11.9
N_c [cm^{-3}]	$2.8x\ 10^{19}$	$2.8x10^{19}$	$2.8x10^{19}$
N_v [cm^{-3}]	$1.04x10^{19}$	$1.04x10^{19}$	$1.04x10^{19}$
μ_e [$cm^2\ VS^{-1}$]	1400	1400	1400
μ_h [$cm^2\ VS^{-1}$]	450	450	450
N_D [cm^{-3}]	0	0	0
N_A [cm^{-3}]	$1.0x10^{20}$	$1.0x10^{16}$	$1.0x10^{20}$

6. Simulation of Tandem Solar Cell

In the tandem setup of mechanically stacked perovskite solar cells, the top cell plays a pivotal role in capturing high-energy photons. In contrast, the bottom c-Si cell specializes in capturing lower-energy photons. The perovskite layer boasts advantageous qualities such as a high absorption coefficient, fast carrier mobility, and affordability, making it a highly promising material for photovoltaic use. Similarly, the c-Si bottom cell has a strong track record in the photovoltaic industry.

The use of a stacked arrangement incorporating both of these materials has resulted in the tandem perovskite solar cell achieving impressive conversion rates, mitigating the limitations of single-junction cells. However, extensive studies are being conducted to analyze the durability and prolonged functionality of perovskite components. The critical aspect of establishing a reliable and scalable manufacturing procedure is crucial for the eventual advancement of mechanically stacked tandem perovskite solar cells into the market.

Using SCAPS-1D, tandem simulation is done. The analysis utilized a two-terminal tandem cell design, where two diodes are connected in series. A crucial aspect of the simulation is ensuring current matching between the two cells. This means that even when the voltage is the sum of the individual cell voltages, the cell with the lower short-circuit current density (Jsc) dictates the overall current limitation.

To achieve current matching, researchers employed the variation in maximum power current density (JMP) or Jsc. To match the current density of the top cell, the thickness of the n+Si layer is varied to attain the same Jsc value.

For the top cell, a thickness of 0.1 µm is considered for $CuSbS_2$, $CsBi_3I_{10}$, and FTO, while a thickness of 0.03 µm is considered for SnO_2. For the bottom cell, the thicknesses considered are 0.1 µm for P+Si, 10 µm for PSi, and 1.61 µm for n+Si. Table 8 compares the simulation results of the standalone cell from the reference to the tandem cell simulation that is investigated here.

Table 8. Results of simulations

Device Structure	V_{oc}	J_{sc}	FF(%)	PCE(%)
Ref [10]	1.29	16.32	84.7	17.82
$CsBi_3I_{10}$ on c-Si (Tandem)	1.77	13.5	77.69	30.8

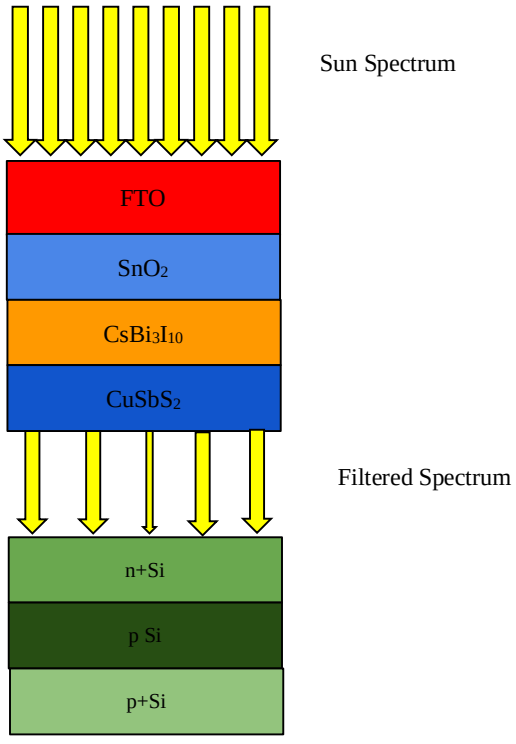

Fig. 14 Proposed a tandem solar cell structure

7. Discussion of the Proposed Structure

Figure 14 depicts the finalized Tandem solar cell considered after optimizing the reference solar cell. Initially, the structure of the glass base PSC is FTO/SnO_2/$CsBi_3I_{10}$/$CuSbS_2$/Au as shown in Figure 1, obtained a PCE of 21.8. However, as evident from Table 8, adjustments are needed to match the Jsc of the upper and lower cells, resulting in a decrease in PCE. The final optimized PSC structure achieved a PCE of 12.29%, maintaining the glass base FTO/SnO_2/$CsBi_3I_{10}$/$CuSbS_2$/Au. The two terminal tandem solar cell is simulated using the optimized top and c-Si bottom cells, and an efficiency of 30.8 was achieved. The increase in efficiency is summarized in Table 8.

8. Conclusion

In a nutshell, the simulation findings highlight the significant potential of $CsBi_3I_{10}$ perovskite solar cells when paired with a c-Si bottom cell in a tandem solar cell arrangement. The research demonstrates how the $CsBi_3I_{10}$ perovskite cell can achieve higher current and voltage levels, resulting in an impressive 21% power conversion efficiency when combined with a c-Si solar cell. This represents a significant improvement compared to both standalone $CsBi_3I_{10}$ perovskite cells and standalone c-Si cells. Additionally, investigating the effect of varying the thickness of the $CsBi_3I_{10}$ layer offers valuable insights. In general, these findings provide encouraging potential for the application of tandem solar cell configurations utilizing CsBi3I10 perovskite solar cells and make a valuable contribution to the advancement of renewable energy in the domains of wind, solar, and wave power.

Acknowledgement

The authors would like to extend their acknowledgement to Gent University, Belgium, for developing and providing the SCAPS-1D simulator used in this work. We would like to express our gratitude to the Visvesvaraya Technological University (VTU) for its support and resources that facilitated the completion of this research paper. Also, we would like to thank P.E.S University, Bengaluru, India, for supporting the work.

References

[1] Bas J. Van Ruijven, Enrica De Cian, and Ian Sue Wing, "Amplification of Future Energy Demand Growth Due to Climate Change," *Nature Communications*, pp. 1-12, 2019. [CrossRef] [Google Scholar] [Publisher Link]

[2] L.L. Yan et al., "A Review on the Crystalline Silicon Bottom Cell for Monolithic Perovskite/Silicon Tandem Solar Cells," *Materials Today Nano*, vol. 7, 2019. [CrossRef] [Google Scholar] [Publisher Link]

[3] Tomas Leijtens et al., "Opportunities and Challenges for Tandem Solar Cells Using Metal Halide Perovskite Semiconductors," *Nature Energy*, pp. 828-838, 2018. [CrossRef] [Google Scholar] [Publisher Link]

[4] Kihwan Kim et al., "Simulations of Chalcopyrite/c-Si Tandem Cells Using SCAPS-1D," *Solar Energy*, vol. 145, pp. 52-58, 2017. [CrossRef] [Google Scholar] [Publisher Link]

[5] Usha Mandadapu, S. Victor Vedanayakam, and K. Thyagarajan, "Simulation and Analysis of Lead Based Perovskite Solar Cell Using SCAPS-1D," *Indian Journal of Science and Technology*, vol. 10, no. 11, pp. 1-8, 2017. [Google Scholar] [Publisher Link]

[6] Jenny A. Nelson, *The Physics of Solar Cells*, World Scientific Publishing Company, pp. 1-384, 2003. [Google Scholar] [Publisher Link]

[7] Simon M. Sze, and Kwok K. Ng, *Physics of Semiconductor Devices*, Wiley, pp. 1-832, 2006. [Google Scholar] [Publisher Link]

[8] Peter Y. Yu, and Manuel Cardona, *Fundamentals of Semiconductors : Physics and Materials Properties*, Springer Berlin, Heidelberg, pp. 1-617, 1996. [Google Scholar] [Publisher Link]

[9] Martin A. Green, *Solar Cells Operating Principles, Technology, and System Applications*, Prentice-Hall, pp. 1-274, 1992. [Google Scholar] [Publisher Link]

[10] Shamim Ahmmed et al., "Performance Analysis of lead-Free $CsBi_3I_{10}$-Based Perovskite Solar Cell through the Numerical Calculation," *Solar Energy*, vol. 226, pp. 54-63, 2021. [CrossRef] [Google Scholar] [Publisher Link]

[11] Bingjuan Zhang et al., "NiO/Perovskite Heterojunction Contact Engineering for Highly Efficient and Stable Perovskite Solar Cells," *Advanced Science*, vol. 7, no. 11, pp. 1-10, 2020. [CrossRef] [Google Scholar] [Publisher Link]

[12] Pandiyarajan Mariyappan et al., "Influence of Inorganic NiO_x Hole Transport Layer on the Growth of $CsBi_3I_{10}$ Perovskite Films for Photovoltaic Applications," *Advanced Materials Interfaces*, vol. 8, no. 7, 2021. [CrossRef] [Google Scholar] [Publisher Link]

[13] I. Chabri et al., "Numerical Analysis of Lead-Free Cs_2SnI_6-Based Perovskite Solar Cell, with Inorganic Charge Transport Layers Using SCAPS-1D" *Journal of Electronic Materials*, vol. 52, pp. 2722-2736, 2023. [CrossRef] [Google Scholar] [Publisher Link]

[14] Faiza Azri et al., "Electron and Hole Transport Layers Optimization by Numerical Simulation of a Perovskite Solar Cell," *Solar Energy*, vol. 181, pp. 372-378, 2019. [CrossRef] [Google Scholar] [Publisher Link]

[15] Jian Kang et al., "Alloying Sb into All Inorganic Lead-Free $CsBi_3I_{10}$ for Improving the Crystal Growth and Photovoltaic Performance," *Journal of Materials Chemistry A*, vol. 10, no. 37, pp. 19618-19625, 2022. [CrossRef] [Google Scholar] [Publisher Link]

[16] M. Khalid Hossain et al., "Combined DFT, SCAPS-1D, and wxAMPS Frameworks for Design Optimization of Efficient Cs_2BiAgI_6-Based Perovskite Solar Cells with Different Charge Transport Layers," *RSC Advances*, vol. 12, no. 54, pp. 34850-34873, 2022. [CrossRef] [Google Scholar] [Publisher Link]

[17] M. Khalid Hossain et al., "Effect of Various Electron and Hole Transport Layers on the Performance of $CsPbI_3$-Based Perovskite Solar Cells: A Numerical Investigation in DFT, SCAPS-1D, and wxAMPS Frameworks," *ACS Omega*, vol. 7, no. 47, pp. 43210-43230, 2022. [CrossRef] [Google Scholar] [Publisher Link]

[18] Lingyan Lin et al., "A Modeled Perovskite Solar Cell Structure with a Cu_2O Hole-Transporting Layer Enabling Over 20% Efficiency by Low-Cost Low-Temperature Processing," *Journal of Physics and Chemistry of Solids*, vol. 124, pp. 205-211, 2019. [CrossRef] [Google Scholar] [Publisher Link]

[19] Lu-Lu Jiang et al., "Interface Engineering Toward Enhanced Efficiency of Planar Perovskite Solar Cells," *Journal of Materials Chemistry A*, vol. 4, no. 1, pp. 217-222, 2016. [CrossRef] [Google Scholar] [Publisher Link]

[20] Zhanglin Guo et al., "High Electrical Conductivity 2D MXene Serves as Additive of Perovskite for Efficient Solar Cells," *Small*, vol. 14, no. 47, 2018. [CrossRef] [Google Scholar] [Publisher Link]

[21] Marwa Sayed Salem Basyoni et al., "On the Investigation of Interface Defects of Solar Cells: Lead-Based vs Lead-Free Perovskite," *IEEE Access*, vol. 9, pp. 130221-130232, 2021. [CrossRef] [Google Scholar] [Publisher Link]

[22] Shambhavi Rai, B.K. Pandey, and D.K. Dwivedi, "Modeling of Highly Efficient and Low Cost $CH_3NH_3Pb(I_{1-x}Cl_x)_3$ Based Perovskite Solar Cell by Numerical Simulation," *Optical Materials*, vol. 100, 2020. [CrossRef] [Google Scholar] [Publisher Link]

[23] Aminreza Mohandes, Mahmood Moradi, and Hamid Nadgaran, "Numerical Simulation of Inorganic $Cs_2AgBiBr_6$ as a Lead-Free Perovskite Using Device Simulation SCAPS-1D," *Optical and Quantum Electronics*, vol. 53, 2021. [CrossRef] [Google Scholar] [Publisher Link]

[24] C. Ulbrich et al., "Matching of Silicon Thin-Film Tandem Solar Cells for Maximum Power Output," *International Journal of Photoenergy*, vol. 2013, pp. 1-7, 2013. [CrossRef] [Google Scholar] [Publisher Link]

[25] M. Bonnet-Eymard et al., "Current Matching Optimization in High-Efficiency Thin-Film Silicon Tandem Solar Cells," *2013 IEEE 39th Photovoltaic Specialists Conference (PVSC)*, Tampa, FL, USA, pp. 184-187, 2013. [CrossRef] [Google Scholar] [Publisher Link]